LASER & PHOTONICS REVIEWS
www.lpr-journal.org

Breaking the Coupling Efficiency–Bandwidth Trade-Off in Surface Grating Couplers Using Zero-Order Radiation

Alejandro Sánchez-Postigo, Robert Halir, J. Gonzalo Wangüemert-Pérez, Alejandro Ortega-Moñux, Shurui Wang, Martin Vachon, Jens H. Schmid, Dan-Xia Xu, Pavel Cheben, and Íñigo Molina-Fernández*

Silicon photonics provides wafer-scale fabrication of densely integrated photonic circuits that are enabling breakthrough applications in datacom, artificial intelligence, and healthcare. The sub-micrometer mode size of silicon waveguides makes efficient coupling to conventional single mode fibers extremely challenging. While advanced surface grating couplers can achieve sub-decibel coupling efficiencies, their operation relies on diffraction phenomena, which intrinsically limit the operational bandwidth. Here a novel type of surface coupler is experimentally demonstrated that overcomes the efficiency-bandwidth limitation of conventional diffraction gratings by harnessing zero-order radiation from a subwavelength metamaterial waveguide to a tilted silicon prism. The device achieves a coupling efficiency above 80% to an SMF-28 fiber in a record 1-dB bandwidth beyond 90 nm, opening new venues for highly efficient broadband fiber-to-chip surface coupling in silicon photonics.

1. Introduction

Silicon photonics enables optical chips with densely integrated high-performance devices that can be fabricated at wafer-scale by leveraging the fabrication infrastructure of well-established microelectronic processes.[1,2] As the demand for integrated optics in telecom and datacom continues to grow,[2] and applications increasingly expand into the fields of metrology,[3] light detection and ranging,[4] quantum signal processing,[5] and biochemical sensing,[6,7] there is a rising demand for devices with smaller insertion losses and broader bandwidths. In this sense, efficient and broadband fiber-to-chip coupling continues to be a major challenge in silicon photonics due to the significant size mismatch between the integrated waveguide (with a typical cross-section of 500 nm × 220 nm) and the standard optical fiber core (with a diameter of 10.4 μm).[8] Edge or end-fire couplers are fiber-chip interfaces that, located at the chip facet, adiabatically adapt the mode sizes. Various types of edge couplers have been proposed, including inverse tapers and multilayer structures,[9,10] as well as subwavelength grating (SWG) metamaterial mode expanders.[11,12] Despite their high coupling efficiency (>80%) and 1-dB bandwidth (>100 nm), these couplers are not suitable for wafer-scale testing, a major drawback that is intrinsic to their placement at the chip facets and that is especially problematic for prototyping. This inconvenience is avoided with surface grating couplers, which allow for anywhere-on-wafer placement and relaxed alignment tolerances.[8] A surface grating coupler is a waveguide with a (quasi)periodic perturbation that produces diffraction out of the chip plane and into an optical fiber that is positioned above the chip.[13] Many design and fabrication techniques have been proposed to maximize the peak coupling efficiency, including reduction of back-reflections,[14–18] directionality enhancement,[17–22] and fiber-grating field overlap optimization (apodization),[22–25] some of them achieving sub-decibel peak coupling efficiencies. However, due to the diffractive behavior of grating couplers, any detuning from this peak wavelength results in a variation in the radiation angle and thus in a degradation of the coupling efficiency.[26] This is commonly expressed as the 1-dB bandwidth, that is, the bandwidth in which the grating coupling efficiency remains above 80% of the peak efficiency. While some attempts on broadening the operational bandwidth have been made,[16,27–29] in 2017 Passoni et al. showed theoretically that there is an intrinsic trade-off between the coupling efficiency and the bandwidth in apodized silicon grating couplers for a given fiber mode size.[30]

A. Sánchez-Postigo, R. Halir, J. G. Wangüemert-Pérez, A. Ortega-Moñux, Í. Molina-Fernández
Departamento de Ingeniería de Comunicaciones, ETSI Telecomunicación, Campus de Teatinos s/n
Universidad de Málaga
Málaga 29071, Spain
E-mail: asp@ic.uma.es

S. Wang, M. Vachon, J. H. Schmid, D.-X. Xu, P. Cheben
Advanced Electronics and Photonics Research Centre
National Research Council Canada
1200 Montreal Rd., Ottawa ON K1A 0R6, Canada

The ORCID identification number(s) for the author(s) of this article can be found under https://doi.org/10.1002/lpor.202000542

DOI: 10.1002/lpor.202000542

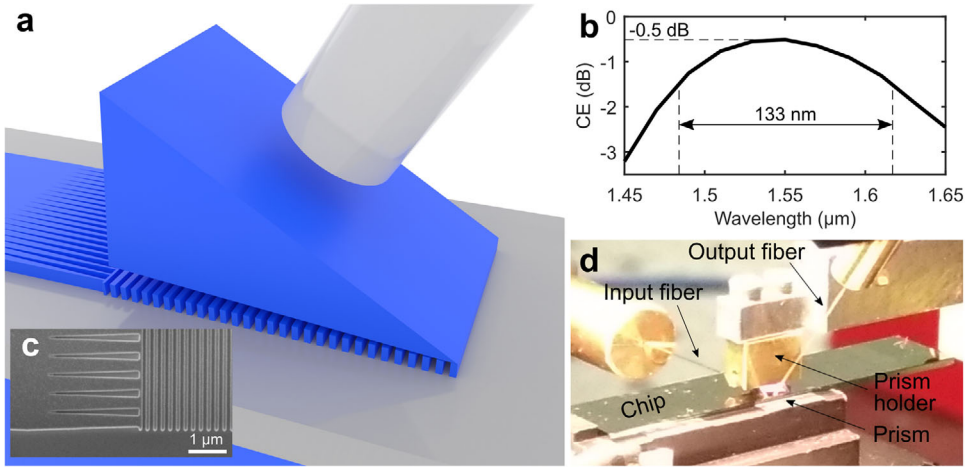

Figure 1. Zero-order grating coupler. a) Schematic representation of the zero-order grating coupler. A subwavelength grating metamaterial waveguide radiates the light from the integrated waveguide toward the optical fiber via a high-refractive-index prism that is placed on top of the structure. The subwavelength segmentation enables bandwidth engineering, while the prism tilt maximizes field overlap, providing a coupling efficiency–bandwidth product beyond 75 nm. This schematic includes the core of an SMF-28 optical fiber and the end section of the input taper, which is used to convert the fundamental mode of the silicon waveguide into the fundamental Bloch–Floquet mode of the subwavelength grating. b) 3D FDTD–simulated coupling efficiency of the coupler as a function of the wavelength. c) SEM image of one of the fabricated gratings (without prism) including part of the input taper on the left-hand side. d) Photograph of the experimental setup (input: facet coupling; output: prism coupling) that was used to characterize the bandwidth of the fabricated zero-order grating coupler, showing the silicon prism held with the appropriate tilt angle on top of the chip.

Thus, the coupling efficiency–bandwidth product (CE·BW) is a natural figure of merit to evaluate the overall performance of surface grating couplers. Apodized, metamaterial-based couplers with bottom mirrors, which are comparatively easy to fabricate, achieve CE·BW ≈ 30 nm,[31] while values up to CE·BW ≈ 60 nm are only achievable with sophisticated layer structuring,[32–34] with plasmonic structures,[35] or using optical fibers with reduced mode field diameter.[33,35]

Here we present the first experimental demonstration of a zero-order silicon surface grating coupler, illustrated in **Figure 1**a, that overcomes the coupling efficiency–bandwidth constraint, without requiring complex fabrication techniques. Our coupler yields a measured spectral 1-dB bandwidth of 94 nm and coupling loss of less than 1 dB, which constitute a record CE·BW beyond 75 nm.

2. Zero-Order Grating Coupling

A schematic representation of a zero-order grating coupler (ZGC) is shown in Figure 1a. The structure comprises a SWG metamaterial waveguide and a silicon prism to extract light from the waveguide into upward radiation. The SWG metamaterial allows for wavelength-dispersion engineering of the grating waveguide and bandwidth optimization.[36,37] The prism is tilted to produce a near-Gaussian radiated field, which maximizes the overlap with the fiber mode without jeopardizing the bandwidth enhancement.

The broadband behavior of the ZGC can be derived from the operation principle of conventional grating couplers (CGCs). The radiation angle θ of light is determined by the phase-matching condition[26]

$$\theta = \sin^{-1}\left(\frac{n_B}{n_u} + m\frac{\lambda}{n_u \Lambda}\right) \quad (1)$$

where n_B is the effective index of the fundamental Bloch–Floquet mode propagating through the grating, n_u is the refractive index of the upper medium into which light is radiated, the integer m is the diffraction order, λ is the wavelength, and Λ is the grating period (pitch). Because $n_B > n_u$, this equation can only be met for real θ when $m < 0$. In this case, Equation (1) shows an explicit relationship between the radiation angle and the wavelength, which is the main reason for the narrow bandwidth of CGCs.[16]

To overcome this limitation, we introduce a pitch Λ such that the periodic waveguide operates below the Bragg threshold (i.e., $\Lambda < 0.5\lambda/n_B$), hence frustrating all diffraction orders. The subwavelength grating effectively behaves as a homogeneous, diffractionless waveguide. As with prism-film couplers,[38,39] radiation can be enabled in the zeroth ($m = 0$) order by placing a high-refractive-index ($n_u > n_B$) material on top of the grating, so that Equation (1) becomes

$$\theta = \sin^{-1}\left(\frac{n_B}{n_u}\right) \quad (2)$$

where the explicit relationship with λ is suppressed, thereby substantially increasing the bandwidth.

In a ZGC, the wavelength limitation arises from the implicit dispersion of n_B and n_u, which depend on the geometry of the waveguide and the upper material, respectively. The minimum SWG dispersion (included in n_B) corresponds to a periodic waveguide operating as far away as possible from the Bragg regime. This operation point can be attained for a duty cycle of 50% and the smallest fabricable grating period, that is, Λ = 2·MFS, where MFS is the minimum feature size of the lithographic process. We considered an MFS of 100 nm, which is compatible with current 193-nm deep-UV lithography.[40] Thus, the grating period is chosen as 200 nm. Additionally, the coupling efficiency is maximized without compromising the bandwidth

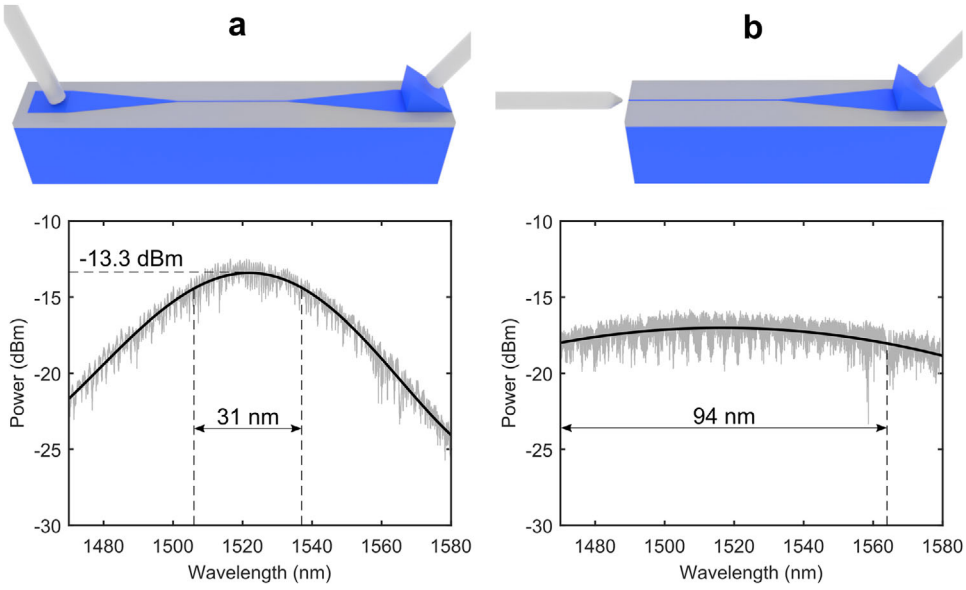

Figure 2. Experimental setups and power spectra at the output of the zero-order grating couplers. a) Experiment 1. Top: Illustration of the experiment: light is injected into the chip using a conventional grating coupler with a limited bandwidth response of ≈30 nm. Bottom: Spectral response (raw data) obtained with Experiment 1, with the same 1-dB bandwidth of ≈30 nm as the conventional grating coupler. b) Experiment 2. Top: Illustration of the experiment: light is injected into the chip through the facet. Bottom: Spectral response (raw data) obtained with Experiment 2, revealing a broad bandwidth for the zero-order grating coupler. The ripples in the responses are attributed to reflections from imperfections in the chip. In both (a) and (b), the light from a laser with an output power of 1 mW (0 dBm) is guided on-chip to the zero-order grating coupler under test, which couples the light out of the chip into an SMF-28 optical fiber. To facilitate the estimation of the 1-dB bandwidth and the peak losses, the responses are fitted with high-order polynomials, which are plotted in a bold black line over the raw data (grey color).

by tilting the prism 1° with respect to the chip plane. The design procedure is described in detail in our previous theoretical paper,[41] while specific structural parameters can be found in the Supporting Information (see Figure S1 and Table S1, Supporting Information). A 3D finite-difference time-domain (3D FDTD) simulation of the nominal configuration, shown in Figure 1b, provides a 1-dB bandwidth of 133 nm and a coupling efficiency of −0.5 dB (89%), yielding a theoretical CE·BW of 118 nm.

To minimize back-reflections, an injection stage is designed that comprises two sections: 1) an adiabatic linear taper to expand the fundamental mode from a narrow 500-nm interconnecting waveguide to a 15-µm wide homogeneous waveguide and 2) a short (3 µm) transition to convert the uniform mode into the Bloch–Floquet mode of the subwavelength grating (see Figure 1a,c). The transition stage consists of a series of transversely periodic trapezoids to match the effective indices at both sides of the section. Detailed structural parameters can be found in the Supporting Information (see Figure S2 and Table S2, Supporting Information).

3. Fabrication

Samples were fabricated on a silicon-on-insulator (SOI) platform with 220-nm silicon layer and 3-µm buried oxide. The waveguide pattern including the grating couplers was defined by electron beam lithography using hydrogen silsesquioxane resist and inductively coupled high density plasma etching with SF_6-C_4F_8 chemistry.

Although ZGCs can indeed be implemented anywhere on the chip surface, to facilitate prism positioning in our measurement setup and to accommodate the fiber cladding, we placed the subwavelength gratings in proximity of the chip's cleaved edges. This little inconvenience can be circumvented by either using custom optical fibers with reduced cladding thickness or etching a deep trench near the ZGC to make room for the standard fiber cladding. Furthermore, the ability to couple light to the chip via cleaved facets helps us to accurately determine broadband characteristics of the coupler. While the nominal gratings are only ≈20 µm long, a grating length of 1 mm was chosen to avoid removing the gratings in the cleaving process, which has a limited positional accuracy. After cleaving, an extraneous grating length of ≈500 µm was left. Due to the prism tilt effect, radiation is only effective in the short region of the grating (≈20 µm) near the prism contact point. A scanning-electron-microscope (SEM) image of one of the fabricated ZGCs is shown in Figure 1c.

A custom silicon prism was procured from LightMachinery Inc.[42] with a base of 2 mm × 2 mm and an angle of 35.7° between the input and output surfaces. The larger prism size compared to the coupler length simplifies prism manipulation and the angle guarantees that light is not refracted at the silicon-air interface when the prism is correctly positioned. The prism is attached from the top to a holder that suspends it in the air and allows accurate positioning, including the tilt adjustment, by a micro-positioning stage (see Figure 1d).

4. Experimental Characterization

Measurements of sub-decibel coupling efficiency and broad bandwidth are challenging, so we set up two independent complementary experiments: In Experiment 1, light is coupled

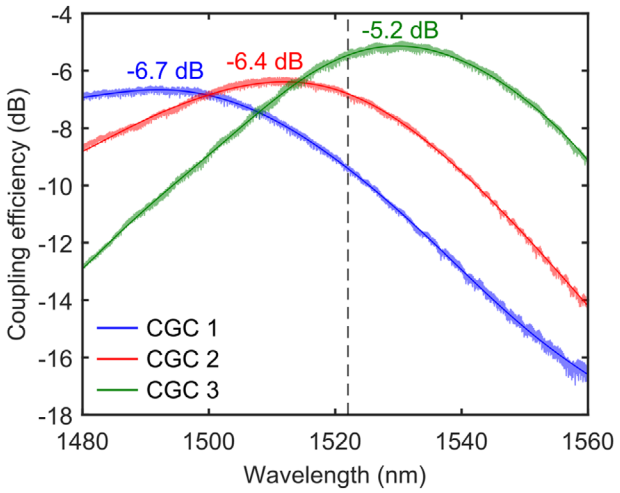

Figure 3. Measured coupling efficiency of conventional grating couplers used for calibration as a function of the wavelength. The 1-dB bandwidth of the conventional grating couplers is ≈30 nm. The dashed line shows the center wavelength of the spectral response that is measured from the experiment in Figure 2a, which uses conventional grating couplers as input interfaces.

into the chip through a previously characterized auxiliary conventional (non-zero-order) grating coupler, travels through a waveguide, and then couples out via a ZGC, as illustrated in **Figure 2**a (top). Since the bandwidth limitation of the conventional coupler hinders the accurate estimation of the bandwidth of the ZGC, we utilize Experiment 2 to determine the bandwidth. Here we couple light into the chip through a cleaved facet; then, the light travels through a waveguide and couples out via a ZGC, as seen in Figure 2b (top). A photograph of this coupling setup is shown in Figure 1d. Another possible option would be to use a prism-to-chip-to-prism coupling, however such a setup is not available in our laboratory.

First, we measured the fiber-to-fiber system loss. Using the cut-back method, we also estimated other losses that need to be accounted for to determine the coupling efficiency of the ZGC. These include the losses of the interconnecting waveguides, homogeneous-to-SWG tapers, and the extraneous length of the SWG waveguides. Then, using a conventional grating-to-grating coupler setup, we measured the spectral responses of the auxiliary (non-zero-order) grating couplers, which were fabricated with several variations in the size of the silicon segments. For these measurements, the optical fiber was positioned at an angle that maximized light coupling. Spectral responses of the CGCs are shown in **Figure 3**, after subtracting additional losses from the system and waveguides.

For Experiment 1, the measured power as a function of the wavelength is shown in Figure 2a, where raw data is represented in grey. The spectral ripple is attributed to imperfections in the chip that produce reflections, including those in the homogeneous-to-SWG transition and the SWG waveguides. Fitted data is highlighted to facilitate spectrum interpretation. The central wavelength determined in this experiment is 1522 nm, suggesting that the conventional input grating coupler is centered near this wavelength. As indicated with the dashed line in Figure 3, other conventional couplers exhibit slightly shifted peak wavelengths, because of dimensional variabilities within the chip due to fabrication deviations. This introduces some uncertainty in determining the peak wavelength and efficiency of the auxiliary conventional coupler used in Experiment 1. Nevertheless, the worst-case coupling efficiency of the ZGC is obtained by considering the best coupling efficiency of the auxiliary coupler, which is −5.2 dB. This yields a worst-case value of the coupling efficiency of the ZGC of -1.0 ± 0.2 dB. A detailed description of the calibration of losses that has been performed to estimate this coupling efficiency can be found in the Experimental Section (Section 7). Furthermore, by interpolating the peak values in Figure 3, a coupling efficiency of −5.7 dB can be estimated for the auxiliary grating coupler at a wavelength of 1522 nm. This predicts an estimated nominal efficiency of −0.5 dB, in excellent agreement with our simulation results.

The 1-dB bandwidth in Experiment 1 spectrum is only 31 nm, which corresponds to the 1-dB bandwidth of the conventional coupler and is consistent with the expected broad bandwidth of the ZGC. To provide an accurate estimation of this metric, we carried out Experiment 2. The measured spectrum resulting from this experiment is shown in Figure 2b and exhibits a broad 1-dB bandwidth of 94 nm, which corresponds to that of the ZGC, since the facet coupling does not limit the bandwidth in this characterization scheme. These experimental results confirm a lower bound for the CE·BW of 75 nm, which is an unprecedented performance for a fiber-chip surface grating coupler.

5. Discussion

The measurements in Experiment 2, which are not affected by auxiliary grating couplers, fundamentally demonstrate the broad spectral response of the ZGC. According to Figure 2b, the peak efficiency is achieved at a wavelength of 1519 nm, which constitutes a shift of 31 nm with respect to the nominal wavelength of 1550 nm. On the other hand, the estimated 1-dB bandwidth is 94 nm, smaller than the designed 133 nm. In order to understand these differences between simulation and experiments, we theoretically study the influence of fiber tilt misalignments and fabrication imperfections on the ZGC's performance.

Figure 4a shows the calculated coupling efficiency as a function of wavelength for several optical fiber tilt angles, using 2D FDTD simulations. It is observed that the central wavelength of the ZGC is sensitive to fiber tilt misalignments, as in CGCs. Specifically, the wavelength shift of 31 nm can be associated to an angular misalignment of 1°, without compromising coupling efficiency or bandwidth. In Figure 4b we show the simulated spectral response of the ZGC for duty cycles of 65% and 35%, that is, fabrication deviations of ±30 nm, respectively. For +30 nm, the 1-dB bandwidth is reduced 22 nm with respect to the nominal value. For a given period, this bandwidth penalty is a consequence of the higher metamaterial refractive index and SWG dispersion. We attribute the difference in bandwidth between design and measurement to these variations in the effective refractive index of the SWG metamaterial structure. We have also studied the tolerance to the prism tilt angle. In Figure 4c, the calculated penalty on the coupling efficiency is shown as a function of the prism tilt angle, φ. For each value of the tilt angle, the optical fiber is slightly realigned to maximize the coupling efficiency. The penalty on coupling efficiency is less than 1 dB

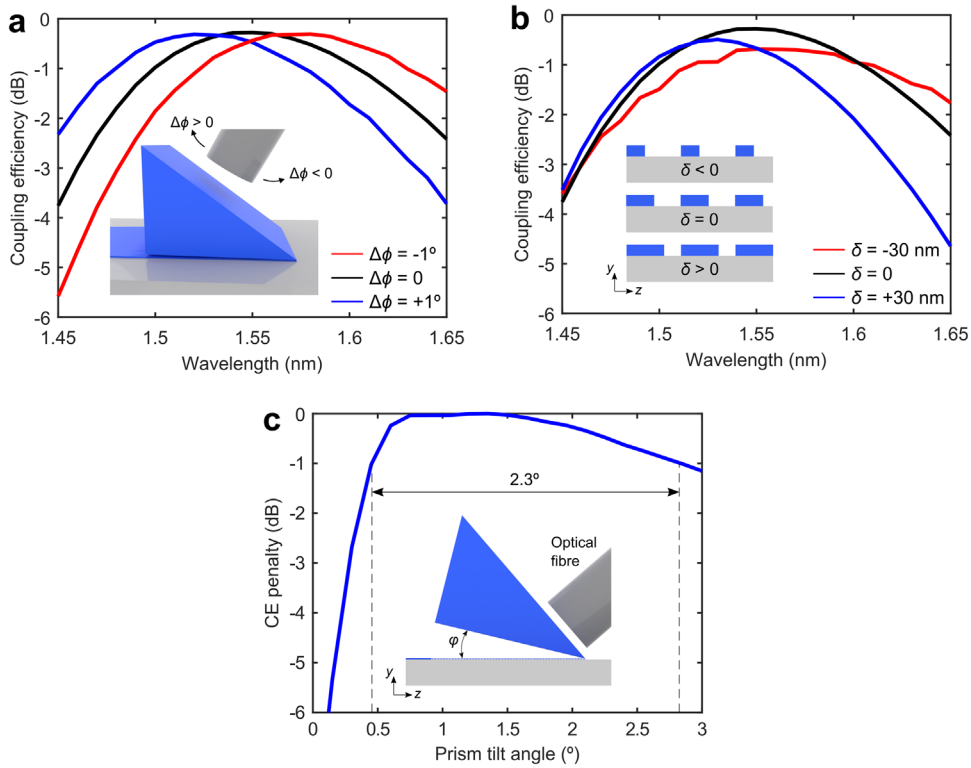

Figure 4. Influence of angular misalignment and fabrication errors on the coupling efficiency, central wavelength, and bandwidth of the measured responses. a) Simulated (2D FDTD) coupling efficiency as a function of wavelength for the optical fiber tilt misalignments of ±1°. Red- and blue-shifts of the central wavelength up to 30 nm are predicted, while the peak coupling efficiency is only minimally affected. b) Simulated (2D FDTD) coupling efficiency as a function of wavelength for fabrication errors of ±30 nm. A positive error means the grating duty cycle is increased. The bandwidth is decreased for positive errors, mainly because of the increase in the SWG dispersion. c) Simulated (2D FDTD) penalty on coupling efficiency as a function of the prism tilt angle, φ.

within a range of prism tilt angles of 0.5°–2.8°. With a tilt control tolerance of ±0.17°, which is easy to achieve with common micro-positioning systems, the prism can be positioned with negligible penalty on coupling efficiency, so that no significant challenges due to prism alignment are expected for prospective applications.

6. Conclusion

We have demonstrated a zero-order surface grating coupler, overcoming the inherent efficiency and bandwidth product limit of state-of-the-art devices. Here the light radiation is not governed by diffraction phenomena as in conventional grating couplers, but by the evanescent tunneling effect between a metamaterial waveguide and a silicon prism placed on top of the chip with a specific tilt angle. We have shown a 1-dB bandwidth broader than 90 nm and a coupling loss of 1 dB or less, yielding the highest CE·BW yet reported for surface couplers, as illustrated in **Figure 5**. Zero-order grating couplers with even broader bandwidths can potentially be developed when fabrication methods with sub 100-nm minimum feature sizes became commonly available in silicon photonics. By leveraging subwavelength metamaterial engineering, this novel surface fiber-chip coupler opens the door for a new library of surface couplers with high performance for future optical communication and interconnects applications.

7. Experimental Section

Simulation: Preliminary designs were performed using our in-house eigenmode expansion simulator, FEXEN, which is specifically optimized for the efficient analysis of periodic structures.[43] FDTD simulations were carried out using Synopsys' Rsoft FullWAVE.[44] For 2D simulations, approximate results were achieved by considering the 2D side view of the grating illustrated in Figure S1, Supporting Information, including the optical fiber and an input taper section that matched the fundamental mode of a homogeneous waveguide with that of the subwavelength grating. For 3D propagation, the full structure was considered. Coupling efficiency and bandwidth were estimated by placing overlap monitors across the optical fiber and scanning the wavelength.

Measurement Setup: For Experiment 1, conventional SMF-28 optical fibers with a 18° polished facet that maximized the coupling of light into the conventional input grating couplers were utilized. For Experiment 2, light was coupled into the chip using lensed polarization-maintaining optical fibers with a mode field diameter of ≈1 μm. In both experiments, a tunable laser with an output power of 1 mW (0 dBm) was used as a light source. Input TE polarization was set by a pigtailed half-wave plate polarization rotator. At the output, the antireflection (AR) coated silicon prism was suspended on top of the chip with a tilt angle of 1° using a mechanical holder mounted on a micro-positioning stage. The light was coupled through the AR-coated prism interface to the cleaved SMF-28 optical fiber and a photodetector.

Calibration of Losses to Estimate the Worst-Case Coupling Efficiency: The power measured in Experiment 1, −13.3 dBm (see Figure 2a), included the coupling loss of the ZGC under test plus a number of losses from various sources, which must be calibrated out. First, the intrinsic loss of the characterization system (i.e., laser—polarization rotator—patch

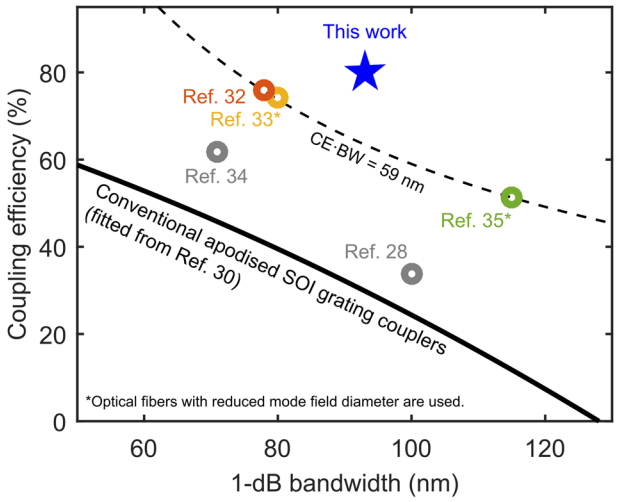

Figure 5. State of the art. Coupling efficiency as a function of the 1-dB bandwidth of several grating couplers reported in the literature. The black curve is a fitting of the Pareto front provided by Passoni et al.[30] and shows the maximum coupling efficiency–bandwidth product (≈35 nm) that is theoretically achievable in conventional, apodized silicon-on-insulator grating couplers designed for standard single-mode optical fibers. The circles correspond to the state-of-the-art surface grating couplers that have been experimentally demonstrated using sophisticated techniques (e.g., multilayering or plasmonics) or using non-SMF-28 optical fibers with reduced mode field diameter, and have a coupling efficiency–bandwidth product exceeding 35 nm. The dashed line identifies the 59-nm coupling efficiency–bandwidth mark, which is the highest performance yet demonstrated in the literature. The star identifies the metric of the device demonstrated in this work, which outperforms all previously reported surface grating couplers.

cord—photodetector) was measured to be 3.9 dB. Using the cut-back method, which normalized the measurements and therefore removed uncertainties due to light coupling through the chip facet, the propagation loss of the interconnecting waveguides and SWG waveguides were calculated, yielding 0.9 dB (0.5 cm × 1.9 dB cm^{-1}) and 1.8 dB (0.5 mm × 3.6 dB mm^{-1}) at a wavelength of 1522 nm, respectively. The latter needed to be subtracted because the 500-μm long subwavelength gratings that were beneath the prism were only a consequence of the specific fabrication process followed in the experiments, but the effective coupling length was only ≈20 μm. Likewise, using a similar procedure, the transmission loss of the homogeneous-to-SWG tapers was estimated to be 0.5 dB.

Finally, for the characterization of the CGCs, a different setup (CGC-to-CGC), with a system loss of 2.0 dB, was utilized. The length of the interconnecting waveguides was 0.7 mm, yielding a propagation loss of 0.1 dB. The measured peak powers were −15.6 dBm (CGC 1), −15.0 dBm (CGC 2), and −12.5 dBm (CGC 3). Assuming that the input and output CGCs were of identical performance, by subtracting the system and waveguide losses and dividing the measured power by two the responses in Figure 3 were obtained. As justified in Section 4, a coupling efficiency of −5.2 dB (CGC 3) was considered as a worst case for the estimation of the ZGC's efficiency.

By subtracting these losses from the measured power from Experiment 1, a worst-case coupling efficiency of −1.0 dB was assessed [−13.3 dBm (Experiment 1 measurement) + 3.9 dB (system losses) + 0.9 dB (waveguide losses) + 1.8 dB (extraneous SWG losses) + 0.5 dB (taper losses) + 5.2 dB (grating coupler losses)].

For this worst-case coupling efficiency, a standard deviation of ±0.2 dB was estimated, which was produced by the uncertainty of the measurement system, the propagation losses of the interconnecting waveguides and the extraneous SWG sections, and the taper loss, as well as the uncertainty associated to the mechanical positioning during the characterization experiment. Details about the determination of the measurement uncertainty can be found in Section B, Supporting Information.

Supporting Information

Supporting Information is available from the Wiley Online Library or from the author.

Acknowledgements

The authors acknowledge funding from Universidad de Málaga, Ministerio de Ciencia, Innovación y Universidades (MCIU) (PID2019-106747RB-I00), Consejería de Economía, Conocimiento, Empresas y Universidad (CECEU) (UMA18-FEDERJA-219, P18-RT-1453, P18-RT-793) and National Research Council of Canada (NRC) Collaborative Science, Technology and Innovation Program (CSTIP) (HTSN 209). The authors would like to thank John Weber from NRC Canada for his help building mechanical support for the prism.

Conflict of Interest

The authors declare no conflict of interest.

Data Availability Statement

The data that support the findings of this study are available from the corresponding author upon reasonable request.

Keywords

fiber-chip coupling, nanophotonic waveguides, on-chip metamaterials, silicon photonics, subwavelength gratings, subwavelength integrated photonics, surface grating couplers

Received: November 28, 2020
Revised: March 3, 2021
Published online: May 5, 2021

[1] X. Chen, M. M. Milosevic, S. Stankovic, S. Reynolds, T. D. Bucio, K. Li, D. J. Thomson, F. Gardes, G. T. Reed, *Proc. IEEE* **2018**, *106*, 2101.
[2] A. H. Atabaki, S. Moazeni, F. Pavanello, H. Gevorgyan, J. Notaros, L. Alloatti, M. T. Wade, C. Sun, S. A. Kruger, H. Meng, K. Al Qubaisi, I. Wang, B. Zhang, A. Khilo, C. V. Baiocco, M. A. Popović, V. M. Stojanović, R. J. Ram, *Nature* **2018**, *556*, 349.
[3] A. Bag, M. Neugebauer, U. Mick, S. Christiansen, S. A. Schulz, P. Banzer, *Nat. Commun.* **2020**, *11*, 2915.
[4] K. Y. Yang, J. Skarda, M. Cotrufo, A. Dutt, G. H. Ahn, M. Sawaby, D. Vercruysse, A. Arbabian, S. Fan, A. Alù, J. Vučković, *Nat. Photonics* **2020**, *14*, 369.
[5] A. W. Elshaari, W. Pernice, K. Srinivasan, O. Benson, V. Zwiller, *Nat. Photonics* **2020**, *14*, 285.
[6] R. Soref, *Nat. Photonics* **2010**, *4*, 495.
[7] J. Juan-Colás, A. Parkin, K. E. Dunn, M. G. Scullion, T. F. Krauss, S. D. Johnson, *Nat. Commun.* **2016**, *7*, 12769.
[8] R. Marchetti, C. Lacava, L. Carroll, K. Gradkowski, P. Minzioni, *Photonics Res.* **2019**, *7*, 201.
[9] M. Papes, P. Cheben, D. Benedikovic, J. H. Schmid, J. Pond, R. Halir, A. Ortega-Moñux, G. Wangüemert-Pérez, W. N. Ye, D.-X. Xu, S. Janz, M. Dado, V. Vašinek, *Opt. Express* **2016**, *24*, 5026.

[10] A. Dewanjee, J. N. Caspers, J. S. Aitchison, M. Mojahedi, *Opt. Express* **2016**, *24*, 28194.
[11] P. Cheben, J. H. Schmid, S. Wang, D.-X. Xu, M. Vachon, S. Janz, J. Lapointe, Y. Painchaud, M.-J. Picard, *Opt. Express* **2015**, *23*, 22553.
[12] T. Barwicz, B. Peng, R. Leidy, A. Janta-Polczynski, T. Houghton, M. Khater, S. Kamlapurkar, S. Engelmann, P. Fortier, N. Boyer, W. M. J. Green, *IEEE J. Sel. Top. Quantum Electron.* **2019**, *25*, 4700313.
[13] D. Taillaert, W. Bogaerts, P. Bienstman, T. F. Krauss, P. Van Daele, I. Moerman, S. Verstuyft, K. De Mesel, R. Baets, *IEEE J. Quantum Electron.* **2002**, *38*, 949.
[14] G. Roelkens, D. Van Thourhout, R. Baets, *Opt. Lett.* **2007**, *32*, 1495.
[15] Y. Li, D. Vermeulen, Y. De Koninck, G. Yurtsever, G. Roelkens, R. Baets, *Opt. Lett.* **2012**, *37*, 4356.
[16] Y. Wang, W. Shi, X. Wang, Z. Lu, M. Caverley, R. Bojko, L. Chrostowski, N. A. F. Jaeger, *Opt. Lett.* **2015**, *40*, 4647.
[17] D. Benedikovic, C. Alonso-Ramos, P. Cheben, J. H. Schmid, S. Wang, D.-X. Xu, J. Lapointe, S. Janz, R. Halir, A. Ortega-Moñux, J. G. Wangüemert-Pérez, I. Molina-Fernández, J.-M. Fédéli, L. Vivien, M. Dado, *Opt. Lett.* **2015**, *40*, 4190.
[18] D. Benedikovic, C. Alonso-Ramos, D. Pérez-Galacho, S. Guerber, V. Vakarin, G. Marcaud, X. L. Roux, E. Cassan, D. Marris-Morini, P. Cheben, F. Boeuf, C. Baudot, L. Vivien, *Opt. Lett.* **2017**, *42*, 3439.
[19] P. Cheben, S. Janz, D. X. Xu, B. Lamontagne, A. Delâge, S. Tanev, *IEEE Photonics Technol. Lett.* **2006**, *18*, 13.
[20] F. Van Laere, G. Roelkens, M. Ayre, J. Schrauwen, D. Taillaert, D. Van Thourhout, T. F. Krauss, R. Baets, *J. Lightwave Technol.* **2007**, *25*, 151.
[21] T. Watanabe, M. Ayata, U. Koch, Y. Fedoryshyn, J. Leuthold, *J. Lightwave Technol.* **2017**, *35*, 4663.
[22] D. Benedikovic, C. Alonso-Ramos, S. Guerber, X. L. Roux, P. Cheben, C. Dupré, B. Szelag, D. Fowler, É. Cassan, D. Marris-Morini, C. Baudot, F. Boeuf, L. Vivien, *Opt. Express* **2019**, *27*, 26239.
[23] R. Halir, P. Cheben, S. Janz, D.-X. Xu, I. Molina-Fernández, J. G. Wangüemert-Pérez, *Opt. Lett.* **2009**, *34*, 1408.
[24] A. Bozzola, L. Carroll, D. Gerace, I. Cristiani, L. C. Andreani, *Opt. Express* **2015**, *23*, 16289.
[25] D. Benedikovic, P. Cheben, J. H. Schmid, D.-X. Xu, B. Lamontagne, S. Wang, J. Lapointe, R. Halir, A. Ortega-Moñux, S. Janz, M. Dado, *Opt. Express* **2015**, *23*, 22628.
[26] T. Tamir, S. T. Peng, *Appl. Phys.* **1977**, *14*, 235.
[27] C. R. Doerr, L. Chen, Y.-K. Chen, L. L. Buhl, *IEEE Photonics Technol. Lett.* **2010**, *22*, 1461.
[28] Q. Zhong, V. Veerasubramanian, Y. Wang, W. Shi, D. Patel, S. Ghosh, A. Samani, L. Chrostowski, R. Bojko, D. V. Plant, *Opt. Express* **2014**, *22*, 18224.
[29] Z. Cheng, X. Chen, C. Y. Wong, K. Xu, H. K. Tsang, *Opt. Lett.* **2012**, *37*, 5181.
[30] M. Passoni, D. Gerace, L. Carroll, L. C. Andreani, *Appl. Phys. Lett.* **2017**, *110*, 041107.
[31] N. Hoppe, W. S. Zaoui, L. Rathgeber, Y. Wang, R. H. Klenk, W. Vogel, M. Kaschel, S. L. Portalupi, J. Burghartz, M. Berroth, *IEEE J. Sel. Top. Quantum Electron.* **2020**, *26*, 1.
[32] W. D. Sacher, Y. Huang, L. Ding, B. J. F. Taylor, H. Jayatilleka, G.-Q. Lo, J. K. S. Poon, *Opt. Express* **2014**, *22*, 10938.
[33] M. T. Wade, F. Pavanello, R. Kumar, C. M. Gentry, A. Atabaki, R. Ram, V. Stojanović, M. A. Popović, *2015 IEEE Opt. Interconnects Conf. OI*, IEEE, Piscataway, NJ **2015**, pp. 46–47.
[34] J. C. C. Mak, Q. Wilmart, S. Olivier, S. Menezo, J. K. S. Poon, *Opt. Express* **2018**, *26*, 13656.
[35] M. Ayata, Y. Fedoryshyn, U. Koch, J. Leuthold, *Opt. Express* **2019**, *27*, 29719.
[36] P. Cheben, R. Halir, J. H. Schmid, H. A. Atwater, D. R. Smith, *Nature* **2018**, *560*, 565.
[37] R. Halir, A. Ortega-Moñux, D. Benedikovic, G. Z. Mashanovich, J. G. Wangüemert-Pérez, J. H. Schmid, Í. Molina-Fernández, P. Cheben, *Proc. IEEE* **2018**, *106*, 2144.
[38] P. K. Tien, R. Ulrich, R. J. Martin, *Appl. Phys. Lett.* **1969**, *14*, 291.
[39] R. Ulrich, *J. Opt. Soc. Am.* **1970**, *60*, 1337.
[40] M. Kamandar Dezfouli, Y. Grinberg, D. Melati, P. Cheben, J. H. Schmid, A. Sánchez-Postigo, A. Ortega-Moñux, G. Wangüemert-Pérez, R. Cheriton, S. Janz, D.-X. Xu, *Opt. Lett.* **2020**, *45*, 3701.
[41] A. Sánchez-Postigo, J. G. Wangüemert-Pérez, J. M. Luque-González, Í. Molina-Fernández, P. Cheben, C. A. Alonso-Ramos, R. Halir, J. H. Schmid, A. Ortega-Moñux, *Opt. Lett.* **2016**, *41*, 3013.
[42] LightMachinery Inc., https://lightmachinery.com/ (accessed: November 2020).
[43] L. Zavargo-Peche, A. Ortega-Moñux, J. G. Wangüemert-Pérez, Í. Molina-Fernández, *Prog. Electromagn. Res.* **2012**, *123*, 447.
[44] FDTD Simulation Software - FullWAVE - Finite Difference Time Domain | RSoft Products, https://www.synopsys.com/photonic-solutions/rsoft-photonic-device-tools/passive-device-fullwave.html, (accessed: November 2020).